Structure-Preserving Constrained Optimal Trajectory Planning of a Wheeled Inverted Pendulum

Klaus Albert, Karmvir Singh Phogat, Felix Anhalt, Ravi N. Banavar, Debasish Chatterjee, and Boris Lohmann

***Abstract*—The wheeled inverted pendulum (WIP) is an underactuated, nonholonomic mechatronic system, and has been popularized commercially as the Segway. Designing a control law for motion planning, that incorporates the state and control constraints, while respecting the configuration manifold, is a challenging problem. In this article, we derive a discrete-time model of the WIP system using discrete mechanics and generate optimal trajectories for the WIP system by solving a discrete-time constrained optimal control problem. Furthermore, we describe a nonlinear continuous-time model with parameters for designing a closed-loop linear–quadratic regulator (LQR). A dual control architecture is implemented in which the designed optimal trajectory is, then, provided as a reference to the robot with the optimal control trajectory as a feedforward control action, and an LQR in the feedback mode is employed to mitigate noise and disturbances for ensuing stable motion of the WIP system. While performing experiments on the WIP system involving aggressive maneuvers with fairly sharp turns, we found a high degree of congruence in the designed optimal trajectories and the path traced by the robot while tracking these trajectories. This corroborates the validity of the nonlinear model and the control scheme. Finally, these experiments demonstrate the highly nonlinear nature of the WIP system and robustness of the control scheme.**

***Index Terms*—Discrete mechanics, geometric control, optimal control, wheeled inverted pendulum (WIP).**

I. Introduction

DESIGNING discrete-time control laws for mechanical systems subject to both state and control constraints, while preserving the configuration manifold of the system, is an extremely challenging problem. Existing control techniques, typically, use trial and error approaches based on prior experience to meet the constraints while the discretization procedure is (somewhat heuristically) a variant of Runge–Kutta fourth order. A scheme for control synthesis in discrete-time that respects the manifold structure and is computationally tractable for the resulting discrete-time system, while respecting the state and control constraints, is most desirable. This problem is addressed and implemented, here, in two steps on the wheeled inverted pendulum (WIP): First, the variational integrator for the mechanical system is derived using discrete mechanics [1] that preserves the manifold structure, and an open-loop control function is obtained by solving a discrete-time constrained optimal control problem using nonlinear programming techniques. Second, the optimal trajectory resulting from this open-loop strategy is tracked via linear–quadratic regulator (LQR), a close-loop tracking controller.

The WIP is a mechatronic system that brings in considerable complexity due to its nonholonomic behavior and underactuation. In this article, we derive a discrete-time model of the nonholonomic WIP system and synthesize an optimal control sequence considering both state and control constraints. The efficacy of the proposed control scheme is demonstrated through experiments.

The WIP (see Fig. 1) consists of a vertical body with two coaxial driven wheels. The system is underactuated since there are fewer actuating mechanisms (the drive on the wheels) than the number of configuration variables. In addition, the system

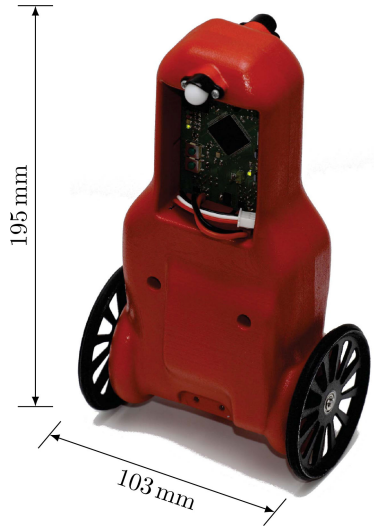

Fig. 1. Picture of the WIP.

Manuscript received October 2, 2019; accepted March 11, 2020. Date of publication May 22, 2020; date of current version June 4, 2020. This work was supported by the TUM Global Alliance Fund administered through Technical University of Munich. The work of K. S. Phogat was supported by the Indian Space Research Organization administered by the ISRO-IITB Cell. This article was recommended for publication by Associate Editor K. Mombaur and Editor E. Yoshida upon evaluation of the reviewers' comments. *(Corresponding author: Klaus Albert.)*

Klaus Albert, Felix Anhalt, and Boris Lohmann are with the Chair of Automatic Control, Department of Mechanical Engineering, Technical University of Munich, 85748 Garching, Germany (e-mail: klaus.albert@tum.de; felix.anhalt@tum.de; lohmann@tum.de).

Karmvir Singh Phogat, Ravi N. Banavar, and Debasish Chatterjee are with the Systems and Control Engineering, Indian Institute of Technology Bombay, Mumbai 400076, India (e-mail: karmvir.p@gmail.com; banavar@iitb.ac.in; dchatter@iitb.ac.in).

This article has supplementary downloadable material available at http://ieeexplore.ieee.org, provided by the authors.

Color versions of one or more of the figures in this article are available online at http://ieeexplore.ieee.org.

Digital Object Identifier 10.1109/TRO.2020.2985579

has nonholonomic constraints that arise due to the pure rolling (without slipping) assumption on the wheels [2], [3] and the no side-slip condition. The WIP finds many applications that include baggage transportation, commuting, and navigation [4]. The system has gained interest in the past several years due to its maneuverability and simple construction (see, e.g., [5], [6]). Other robotic systems based on the WIP are fast becoming popular as well in the robotics community for human assistance and transportation as can be seen in the works of [7]–[10], and a commercially available model Segway for human transportation [4]. Various linear and nonlinear control techniques have been applied to the WIP ranging from LQR [11]–[14] to partial feedback linearization-based nonlinear control [2], vision-based tracking controller using partial feedback linearization [15], and vision-based leader following control using adaptive control techniques [16]. A controllability analysis for the WIP kinematics is presented in [17] and filtering techniques to prevent the WIP leading to limit cycle while stabilizing are discussed in [18]. Recently, a nonlinear position and velocity stabilization controller using energy shaping technique has been proposed in [19], and modeling of the WIP as a linear system with time delays and its stabilization using an integral slide mode control may be found in [20]. A fairly detailed overview of the WIP modeling with various stabilization and tracking control techniques may be found in [7]. Existing control techniques mainly focus on stabilization of the system using some variant of linearization. These control techniques are inapplicable during aggressive and constrained maneuvers due to the fact that these techniques do not consider state and control constraints. Therefore, in challenging scenarios, the performance of these control schemes remains questionable. Note that the WIP models available in literature (see, e.g., [2], [3], [21]) consider torques as control inputs instead of the physical inputs (voltage available to dc motors). During constrained motion planning scenarios, it is essential to consider voltage and current restrictions at the trajectory design stage, which necessitates the modeling of the motor dynamics. A constrained path planning of WIP using variational techniques, in [22], discusses WIP modeling without current dynamics, in which the motor torque is considered as the input, and the system does not account for motor current and voltage restrictions in trajectory planning. In this article, we address this issue by deriving a model of the WIP with motor dynamics in both continuous and discrete time for constrained path planning. Moreover, we conduct experiments to demonstrate efficacy of the proposed scheme unlike [22]. In contrast to our technique, constrained motion planning problems in the stochastic framework is studied extensively in [23] and [24] and references therein. However, these motion planning techniques employ dynamic programming principles for optimal control synthesis, which limits their applicability to high-dimensional systems due to the curse of dimensionality.

Our proposed technique differs from existing control techniques on the following accounts. A variational integrator is proposed that preserves the manifold structure, and in turn, it leads to accurate optimal trajectory design. In addition, we have included the motor dynamics of the system at the design stage to arrive at an accurate nonlinear model. In contrast to various stabilizing controllers proposed in literature, the main thrust of this article lies in the implementation of constrained reachability maneuvers on the WIP. We demonstrate through experiments that the proposed control technique for constrained maneuvers of WIP is efficient and easy to implement.

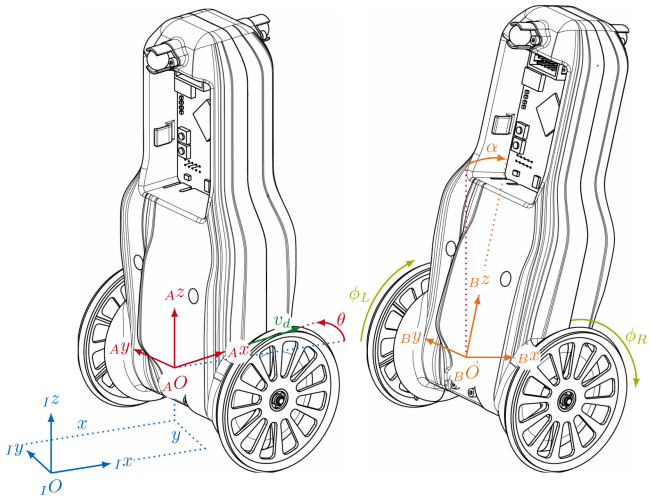

Fig. 2. Coordinate systems and parameters of the WIP.

The article unfolds as follows. We present the model of the WIP system in Section II. Section III-A presents the discrete variational integrator of the WIP, and an optimal control problem is posed in discrete time and solved using a nonlinear solver in Section III-B and its computation time under various schemes is discussed in Section III-C. Section IV is dedicated to setup description with system parameters and followed by results and experiments.

A fairly detailed overview of nonholonomic systems in a geometric framework, in particular the nonholonomic connection, that bears particular relevance to the discrete Lagrange-D'Alembert-Pontryagin (LDAP) principle for deriving variational integrator of WIP is presented in Appendix A to Appendix B. Nonlinear continuous-time WIP model and its discretization is discussed in Appendix C and Appendix D, and design of the LQR and observer may be found in Appendix E.

II. WIP Modeling

A. Continuous-Time Modeling of WIP

The WIP consists of a body of mass m_b mounted on wheels of radius r_w and at a height l from the wheels axis of rotation. A pair of wheels, of mass m_w each, are mounted at the base of the body with a distance $2d_w$ between them, and these wheels are able to rotate independently. The actuating mechanisms of the system, typically two separate motors, are fitted on the body in order to rotate the individual wheels and generate the tilting motion in the system. For these type of systems, one of the control objectives is to steer the system from a given initial configuration on x-y plane to a given final configuration with its body stabilized in the upward position.

The configuration variables (see Fig. 2) of the system are as follows:

1) $(x, y) \in \mathbb{R}^2$: the coordinates of the origin of the body-fixed frame in the horizontal plane of the inertial frame;

2) $\theta \in \mathbb{S}^1$: the heading angle (angle of the wheel rotation axis with the x-axis or the y-axis in the inertial frame);
3) $\alpha \in \mathbb{S}^1$: the tilt angle of the body (angle of the body z-axis with the vertical plane in the inertial frame);
4) $\phi_R \in \mathbb{S}^1$ and $\phi_L \in \mathbb{S}^1$: the relative rotations of the individual wheels w.r.t. the body-fixed frame about the rotation axes of the corresponding wheels;
5) $\mathfrak{q}_R \in \mathbb{R}$ and $\mathfrak{q}_L \in \mathbb{R}$: the charge on the right and left motor terminals. Their time derivatives are the currents flowing through the circuit of right and left electric motors fitted onboard to deliver torque to the wheels.

Based on this choice, the configuration space of the system is

$$Q := \mathrm{SE}(2) \times \mathbb{S}^1 \times \mathbb{S}^1 \times \mathbb{S}^1 \times \mathbb{R} \times \mathbb{R}$$

with a state represented as

$$q := (x, y, \theta, \alpha, \phi_R, \phi_L, \mathfrak{q}_R, \mathfrak{q}_L) \in Q.$$

In sequel, standard geometric notions associated with the manifold Q are: TQ defines the tangent bundle of Q, and T_qQ and T_q^*Q are the tangent space and cotangent space of the manifold Q at q, respectively.

The system is subject to nonholonomic constraints that arise due to no-slip conditions on the wheels, i.e., no lateral sliding and only pure rotation without slipping. Let $(x_L, y_L) \in \mathbb{R}^2$ be the left wheel's position and $(x_R, y_R) \in \mathbb{R}^2$ be the right wheel's position on the x-y plane in the spatial coordinates. Let $\mathbb{R} \ni t \mapsto q(t) \in Q$ denote a system trajectory. Then, the pure rolling motion of the system is given by

$$\begin{cases} \dot{x}_R(t)\cos\theta(t) + \dot{y}_R(t)\sin\theta(t) = r_w\dot{\phi}_R(t) \\ \dot{x}_L(t)\cos\theta(t) + \dot{y}_L(t)\sin\theta(t) = r_w\dot{\phi}_L(t) \end{cases} \tag{1}$$

and the no side-slip constraints are given by

$$\begin{cases} -\dot{x}_R(t)\sin\theta(t) + \dot{y}_R(t)\cos\theta(t) = 0 \\ -\dot{x}_L(t)\sin\theta(t) + \dot{y}_L(t)\cos\theta(t) = 0 \end{cases}. \tag{2}$$

The left- and the right-wheel's positions are defined in terms of the configuration variables in the spatial frame by

$$x_L(t) := x(t) - d_w\sin\theta(t), \quad y_L(t) := y(t) + d_w\cos\theta(t)$$
$$x_R(t) := x(t) + d_w\sin\theta(t), \quad y_R(t) := y(t) - d_w\cos\theta(t).$$

For a system trajectory $\mathbb{R} \ni t \mapsto q(t) \in Q$, the pure rolling constraints (1) and no side-slip constraints (2) are defined in the configuration space by

$$\begin{aligned} \dot{x}(t)\cos\theta(t) + \dot{y}(t)\sin\theta(t) + d_w\dot{\theta}(t) - r_w\dot{\phi}_R(t) = 0 \\ \dot{x}(t)\cos\theta(t) + \dot{y}(t)\sin\theta(t) - d_w\dot{\theta}(t) - r_w\dot{\phi}_L(t) = 0 \\ -\dot{x}(t)\sin\theta(t) + \dot{y}(t)\cos\theta(t) = 0 \end{aligned} \tag{3}$$

which are written in the compressed form as

$$\begin{aligned} \dot{x}(t) - \frac{r_w}{2}\cos\theta(t)\left(\dot{\phi}_R(t) + \dot{\phi}_L(t)\right) &= 0 \\ \dot{y}(t) - \frac{r_w}{2}\sin\theta(t)\left(\dot{\phi}_R(t) + \dot{\phi}_L(t)\right) &= 0 \\ \dot{\theta}(t) - \frac{r_w}{2d_w}\left(\dot{\phi}_R(t) - \dot{\phi}_L(t)\right) &= 0. \end{aligned} \tag{4}$$

We now derive the Lagrangian and the external forcing of the WIP system.

1) Lagrangian of the WIP: In order to define the Lagrangian of the system, let us calculate its kinetic energy T and potential energy V. We start by independently calculating the kinetic energy of each subsystem. Let v_b be the translational velocity of the center of mass and ω_b be the angular velocity of the body with $I_B := \mathrm{diag}(I_{Bxx}, I_{Byy}, I_{Bzz})$ as the inertia of the main body with respect to its center of mass in the body-fixed frame. Then, the kinetic energy of the main body is given by

$$T_b(q, \dot{q}) = \frac{1}{2}(m_b v_b^\intercal v_b + \omega_b^\intercal I_B \omega_b)$$

where

$$v_b := \begin{pmatrix} \dot{x} + l\dot{\alpha}\cos\alpha\cos\theta - l\dot{\theta}\sin\alpha\sin\theta \\ \dot{y} + l\dot{\alpha}\cos\alpha\sin\theta + l\dot{\theta}\sin\alpha\cos\theta \\ -l\dot{\alpha}\sin\alpha \end{pmatrix}$$

and

$$\omega_b := \begin{pmatrix} -\dot{\theta}\sin\alpha, & \dot{\alpha}, & \dot{\theta}\cos\alpha \end{pmatrix}^\intercal.$$

Analogously, to calculate the kinetic energy of the wheels, let $v_{w,R}, v_{w,L}$ be the translational velocity of the right and the left wheel's center of mass, respectively, and let $\omega_{w,R}, \omega_{w,L}$ be the angular velocity of the wheels with $I_W := \mathrm{diag}(I_{Wxx}, I_{Wyy}, I_{Wzz})$ the inertia of the wheels with respect to its center of mass in the body-fixed frame. Then, the kinetic energy of the wheels is given by

$$\begin{aligned} T_w(q, \dot{q}) = &\frac{1}{2}(m_w v_{w,R}^\intercal v_{w,R} + \omega_{w,R}^\intercal I_W \omega_{w,R}) \\ &+ \frac{1}{2}(m_w v_{w,L}^\intercal v_{w,L} + \omega_{w,L}^\intercal I_W \omega_{w,L}) \end{aligned}$$

where

$$v_{w,L} = \begin{pmatrix} \dot{x} - d_w\dot{\theta}\cos\theta \\ \dot{y} - d_w\dot{\theta}\sin\theta \\ 0 \end{pmatrix} \quad \text{and} \quad v_{w,R} = \begin{pmatrix} \dot{x} + d_w\dot{\theta}\cos\theta \\ \dot{y} + d_w\dot{\theta}\sin\theta \\ 0 \end{pmatrix}.$$

We know that the electric motors and the gears rotate at different angular speeds compared to the wheels. Therefore, the rotational energy arising from their relative motion with respect to the body has to be calculated in addition to the above. Let n_{wg} be the transmission ratio from wheel shaft to the gear shaft and n_{wm} be the transmission ratio from the wheel shaft to the motor shaft. The kinetic energy terms due to the relative motion of the gears and the rotor are given by

$$\begin{aligned} T_g(q, \dot{q}) = &\frac{1}{2}I_M(\dot{\alpha} + n_{wm}(\dot{\phi}_R - \dot{\alpha}))^2 \\ &+ \frac{1}{2}I_G(\dot{\alpha} - n_{wg}(\dot{\phi}_R - \dot{\alpha}))^2 \\ &+ \frac{1}{2}I_M(\dot{\alpha} + n_{wm}(\dot{\phi}_L - \dot{\alpha}))^2 \\ &+ \frac{1}{2}I_G(\dot{\alpha} - n_{wg}(\dot{\phi}_L - \dot{\alpha}))^2 \end{aligned}$$

where I_M and I_G are the moments of inertia of the rotor and the gear about their rotation axis, respectively. To incorporate the motor dynamics, the kinetic energy of motor circuits [25] is defined by

$$T_m(q,\dot{q}) = \frac{1}{2}L_m(\dot{\mathfrak{q}}_R^2 + \dot{\mathfrak{q}}_L^2)$$

where L_m is the rotor inductance. Therefore, the total kinetic energy of the system is given by

$$T = T_b + T_w + T_g + T_m.$$

The potential energy of the system is due to the gravitational potential of the body and the potential due to the back EMF of the motor circuits, given by

$$V(q,\dot{q}) = m_b g l\cos\alpha + k_e n_{wm}\big((\dot{\phi}_R - \dot{\alpha})\mathfrak{q}_R + (\dot{\phi}_L - \dot{\alpha})\mathfrak{q}_L\big)$$

where g is the earth gravity and k_e is the motor back EMF constant. The Lagrangian of the WIP is the total kinetic energy minus the potential energy

$$TQ \ni (q,\dot{q}) \mapsto L(q,\dot{q}) = T(q,\dot{q}) - V(q,\dot{q}) \in \mathbb{R}. \tag{5}$$

2) Dissipative and External Forces: The generalized dissipative forces are friction forces between the robot body and the wheels. These forces arise from the gears, the bearing, and the motors losses due to the resistive elements. Let F_{fric} be the dissipative force applied along the generalized coordinates (α, ϕ_R, ϕ_L) and is given by

$$F_{\text{fric}}(q,\dot{q}) := \Big(\text{fric}_R + \text{fric}_L, \quad -\text{fric}_R, \quad -\text{fric}_L\Big)^\intercal$$

where

$$\text{fric}_R := d_v(\dot{\phi}_R - \dot{\alpha}) + d_c\tanh\Big(d_0(\dot{\phi}_R - \dot{\alpha})\Big)$$

and

$$\text{fric}_L := d_v(\dot{\phi}_L - \dot{\alpha}) + d_c\tanh\Big(d_0(\dot{\phi}_L - \dot{\alpha})\Big).$$

The friction losses of the gears and bearing are obtained by identifying the damping parameter d_v, d_c, and d_0 of a typical Coulomb and viscous friction curve from experimental data. Let R_m be the resistance of the motor circuit. The potential drop in the motor circuits due to the resistance is the dissipative force along the generalized coordinates $\mathfrak{q}_L, \mathfrak{q}_R$, and is given by

$$F_{\text{loss}}(q,\dot{q}) := \Big(-R_m\dot{\mathfrak{q}}_R, \quad -R_m\dot{\mathfrak{q}}_L\Big)^\intercal.$$

The external force applied to the system is the voltage available to the motors by the batteries. Let u_R, u_L be the voltage supplied by the batteries to right and left motors, respectively. Therefore, the external force applied along the generalized coordinates $(\mathfrak{q}_L, \mathfrak{q}_R)$ is given by

$$F_{\text{ext}}(u_R,u_L) := (u_R,\ u_L)^\intercal.$$

The net dissipative force and external force applied to the system is given by

$$\mathcal{F}(q,\dot{q},u_R,u_L) = \begin{pmatrix} F_{\text{fric}}(q,\dot{q}) \\ F_{\text{loss}}(q,\dot{q}) + F_{\text{ext}}(u_R,u_L)\end{pmatrix}. \tag{6}$$

A detailed discussion on the derivation of the nonlinear continuous-time model of the WIP is provided in Appendix C.

B. Discrete Mechanics Modeling of WIP

Let us first derive key geometric concepts such as reduced Lagrangian and nonholonomic connection for the WIP, and then apply the LDAP principle (see Appendix B for details) to derive a variational integrator of WIP.

To establish that the WIP is a principle kinematic system, let us define a group action and prove that the vertical space and the constrained distribution at a given configuration have only zero in common; an overview is given in Appendix A. With $G = \text{SE}(2)$ as the Lie group, the configuration space Q of the WIP system can be written in the *trivial bundle* form as

$$Q = G \times M := \text{SE}(2) \times \big(\mathbb{S}^1 \times \mathbb{S}^1 \times \mathbb{S}^1 \times \mathbb{R} \times \mathbb{R}\big)$$

where M is the base space. Therefore, with $s := (\alpha, \phi_L, \phi_R, \mathfrak{q}_R, \mathfrak{q}_L) \in M$ and $g := (x, y, \theta) \in G$, the system configuration is defined by $q := (g, s) \in Q$, and a tangent vector at q is defined by

$$v_q = (v_g, v_s) \in T_qQ$$

where $v_g := (v_x, v_y, v_\theta)$ and $v_s := (v_\alpha, v_{\phi_R}, v_{\phi_L}, v_{\mathfrak{q}_R}, v_{\mathfrak{q}_L})$. In addition, let $\mathfrak{g}$ be the Lie algebra of the Lie group G and $\text{e} : \mathfrak{g} \to G$ be the exponential map[1] from the Lie algebra $\mathfrak{g}$ to the Lie group G. The geometric notions associated with discrete-time WIP modeling are summarized as follows.

1) *Group action (see Appendix A):* The map $\Phi : G \times Q \to Q$ is the group action of the Lie group G on the manifold Q and for $\bar{g} := (X, Y, \Theta) \in G$, the group action Φ is defined (in coordinates) by

$$\begin{aligned}\Phi_{\bar{g}}(q) = \ &(X + x\cos\Theta - y\sin\Theta, Y + x\sin\Theta \\ &+ y\cos\Theta, \Theta + \theta, \alpha, \phi_R, \phi_L, \mathfrak{q}_R, \mathfrak{q}_L).\end{aligned} \tag{7}$$

2) *Vertical Space (see Appendix A):* The vertical space for the system is given by

$$\begin{aligned}\mathcal{V}_q = \Bigg\{ \frac{d}{d\epsilon}\bigg|_{\epsilon=0} (\gamma_\xi(\epsilon), s) \ \bigg|\ \gamma_\xi(0) = g, \\ \dot{\gamma}_\xi(0) = v_g,\ s \in M\Bigg\} \\ = \{(v_g, 0) \in T_gG \times T_sM\}.\end{aligned}$$

For a given local representation of the tangent vectors $v_g := (v_x, v_y, v_\theta) \in T_gG$, the local basis of the vertical space $\mathcal{V}_q$ is given by

$$\mathcal{V}_q = \text{span}\left\{\frac{\partial}{\partial x}, \frac{\partial}{\partial y}, \frac{\partial}{\partial\theta}\right\}.$$

3) *Constrained distribution:* The distribution $\mathcal{D}$ satisfying nonholonomic constraints (4) is called the constrained distribution. The local generator (a collection of linearly independent vector fields spanning the distribution) of the

[1]The exponential map $\text{e} : \mathfrak{g} \to G$ is a local diffeomorphism at $0 \in \mathfrak{g}$.

constrained distribution $\mathcal{D}_q$ satisfying the nonholonomic constraints (4) is given by

$$\mathcal{D}_q = \text{span}\{\mathcal{X}_1, \mathcal{X}_2, \mathcal{X}_3\}$$

where

$$\mathcal{X}_1 = \cos\theta\frac{\partial}{\partial x} - \sin\theta\frac{\partial}{\partial y} + \frac{1}{r_w}\frac{\partial}{\partial \phi_R} + \frac{1}{r_w}\frac{\partial}{\partial \phi_L}$$
$$\mathcal{X}_2 = \frac{\partial}{\partial \alpha}, \quad \mathcal{X}_3 = \frac{\partial}{\partial \theta} + \frac{d_w}{r_w}\frac{\partial}{\partial \phi_R} - \frac{d_w}{r_w}\frac{\partial}{\partial \phi_L}.$$

Thus, it can be seen that

$$\mathcal{S}_q := \mathcal{V}_q \cap \mathcal{D}_q = \{0\}.$$

The class of systems for which $\mathcal{S}_q = \{0\}$ falls into a special category, known as *principal kinematic systems*, in which the tangential directions along the group symmetry are independent of the constrained (due to nonholonomic constraints) tangential directions [26].

1) Reduced Lagrangian: The tangent lift of the group action $\Phi_{\bar{g}}$ is defined in coordinates by

$$T_q\Phi_{\bar{g}}(v_q) = (v_x\cos\Theta - v_y\sin\Theta, v_x\sin\Theta + v_y\cos\Theta, v_\theta, v_\alpha, v_{\phi_R}, v_{\phi_L}, v_{\mathfrak{q}_R}, v_{\mathfrak{q}_L}). \quad (8)$$

Let $TM \times \mathfrak{g} \ni (s, v_s, \xi) := (\Phi_{g^{-1}}(q), T_q\Phi_{g^{-1}}(v_q))$ be a point on the reduced space, where

$$\xi := (v_x\cos\theta + v_y\sin\theta, -v_x\sin\theta + v_y\cos\theta, v_\theta) \quad (9a)$$
$$v_s := (v_\alpha, v_{\phi_R}, v_{\phi_L}, v_{\mathfrak{q}_R}, v_{\mathfrak{q}_L}). \quad (9b)$$

Then, the reduced Lagrangian is defined by

$$TM \times \mathfrak{g} \ni (s, v_s, \xi) \mapsto L^\flat(s, v_s, \xi) := L\left(\Phi_{g^{-1}}(q), T_q\Phi_{g^{-1}}(v_q)\right) \in \mathbb{R}. \quad (10)$$

2) Local Nonholonomic Connection: With our current convention, the $\dot{q}(t) \in T_qQ$ is defined by

$$\dot{q}(t) = \left(\dot{x}(t), \dot{y}(t), \dot{\theta}(t), \dot{\alpha}(t), \dot{\phi}_R(t), \dot{\phi}_L(t), \dot{\mathfrak{q}}_R(t), \dot{\mathfrak{q}}_L(t)\right) := (v_x, v_y, v_\theta, v_\alpha, v_{\phi_R}, v_{\phi_L}, v_{\mathfrak{q}_R}, v_{\mathfrak{q}_L})$$

and further, substituting the value of v_x, v_y, v_θ from (4) into (9a) we obtain the local form of the nonholonomic connection as

$$\xi + \mathbb{A}v_s = 0$$

where

$$\mathbb{A} = \frac{1}{2}\begin{pmatrix} 0 & -r_w & -r_w & 0 & 0 \\ 0 & 0 & 0 & 0 & 0 \\ 0 & -\frac{r_w}{d_w} & \frac{r_w}{d_w} & 0 & 0 \end{pmatrix}. \quad (11)$$

3) Discrete-Time Control Forcing: In a standard way, the control forcing (6) is defined in discrete time as

$$\mathbb{N}_0 \ni k \mapsto \mathcal{F}_k := \mathcal{F}\big(q(t_k), v_q(t_k), u_R(t_k), u_L(t_k)\big) \in T^*M \quad (12)$$

where $\mathbb{N}_0$ is the set of natural numbers including zero.

Collecting the definitions of the reduced Lagrangian (10), the local form of the nonholonomic connection (11), and the discrete-time control force (12), we now apply the LDAP principle (see Appendix B for details) to arrive at a variational integrator of the WIP.

III. Trajectory Planning of the WIP

In order to do trajectory planning in discrete time, we apply tools from discrete mechanics to derive a discrete-time variational integrator[2] and define an optimal control problem in discrete time to synthesize an optimal trajectory.

A. Variational Integrator of WIP

We launch directly into a discrete-time model of the WIP. Let $[N] := \{0, \ldots, N\}$ with a fixed natural number N, A^* be the adjoint of the linear operator A. The right translated tangent lift of the local diffeomorphism e^{-1} at $\zeta \in G$ is defined by

$$\mathfrak{g} \ni \chi \mapsto T\,\mathrm{e}^{-1}(\zeta)\zeta\chi \in \mathfrak{g}$$

where $\chi := \zeta^{-1}\delta\zeta$ and $\delta\zeta \in T_\zeta G$. Let us define a path in discrete time on the configuration space $Q := G \times M$ as

$$[N] \ni k \mapsto (s_k, v_{s_k}, g_k) := (s(t_k), v_s(t_k), g(t_k)) \in TM \times G$$

and derive a variational integrator of WIP by applying the LDAP principle (see Appendix B). The variational integrator for the WIP for the reduced Lagrangian $L^\flat$ (10), local form of the connection $\mathbb{A}$ (11), and the discrete control force $\mathcal{F}$ (12) is given by

$$g_{k+1} = g_k\,\mathrm{e}(-h\mathbb{A}(s_k)v_{s_k}) \quad (13a)$$
$$s_{k+1} = s_k + hv_{s_k} \quad (13b)$$
$$\frac{\partial L_k^\flat}{\partial v_s} - h\frac{\partial L_k^\flat}{\partial s} - \left(D\,\mathrm{e}^{-1}(-v_{s_k}) \circ \mathbb{A}(s_k)\right)^*\left(\frac{\partial L_k^\flat}{\partial \xi}\right) = \frac{\partial L_{k-1}^\flat}{\partial v_s} - \left(D\,\mathrm{e}^{-1}(v_{s_{k-1}}) \circ \mathbb{A}(s_{k-1})\right)^*\left(\frac{\partial L_{k-1}^\flat}{\partial \xi}\right) + h\mathcal{F}_{k-1} \quad (13c)$$

where $h > 0$ is the step length,

$$D\,\mathrm{e}^{-1}(v_{s_k}) := T\,\mathrm{e}^{-1}(\mathrm{e}(-h\mathbb{A}(s_k)v_{s_k})) \circ \mathrm{e}(-h\mathbb{A}(s_k)v_{s_k})$$

and

$$L_k^\flat := L^\flat\left(s_k, (s_{k+1} - s_k)/h, \mathrm{e}^{-1}(g_k^{-1}g_{k+1})/h\right).$$

A few comments are in order here. Equation (13a) governs the update of the system orientation and translation in the x-y plane for a motion in the base space M, (13b) provides the update of the tilt, wheel angles, and the charge at the motor ends, and (13c) describes the dynamics on M. The calculations involved in the discrete-time model are as follows.

Let (g_k, s_k, v_{s_k}) be the states of the system at a discrete instant k. Then, the state at the $(k+1)$th instant is computed in the following manner.

1) Compute the group (orientation and position of the system in x-y plane) update g_{k+1} using (13a) for given g_k and v_{s_k}.

[2]A few modeling inaccuracies reported in [22] are being rectified in this submission.

2) Compute the base configuration update s_{k+1} using (13b) for given s_k and v_{s_k}.
3) If one substitutes s_{k+1} from (13b) in (13c), then (13c) is an implicit form in $v_{s_{k+1}}$ for given states v_{s_k}, s_k and control torque $\mathcal{F}_k$. This implicit form is further solved using Newton's root finding algorithm.

Remark 1: For the sake of completeness, we have described the abovementioned procedure for computing the WIP states using the variation integrator (13). However, during optimization, the variational integrator (13) is treated directly as an equality constraint.

The preceding discussion provides a discrete-time model of the controlled WIP. We move to a constrained optimal control problem in the context of (13).

B. Energy-Optimal Trajectory Planning

The system dynamics, shown previously, is nonlinear.[3] Our objective is to generate an optimal trajectory of the system that passes through prespecified points at predefined times while respecting state and control constraints along the way. Conventional path planning algorithms lack the ability to accommodate state and control constraints at the trajectory design stage while simultaneously minimizing a performance measure. In the technique proposed here, we design a constrained discrete-time optimal trajectory for the WIP system accounting for both state and control constraints that are essential for fast nonlinear dynamics and safety critical systems. The constrained optimal trajectory designed offline is then tracked via an LQR fine-tuned for the discrete-time model derived for the WIP system around zero. The dual controller architecture adopted here is better than conventional schemes due to the fact that it reduces the online computation time and is easy to implement.

We design a constrained trajectory by solving a discrete-time constrained optimal control problem in which the variational integrator of the WIP accounts for the system dynamics. This integrator is employed for the trajectory generation due to the fact that it is more accurate than conventional integration techniques [27], and it preserves system invariants like momentum, energy, etc. The optimal control objective is then to design an energy minimizing path to transport the WIP from a given fixed initial state to a given final state passing through $N_m \leq N$ prespecified configurations $\{\bar{g}_{k_j}\}_{k_j=1}^{N_m} \subset G$ and satisfying the following state and control constraints throughout its journey:

c-i) input voltage (u_R, u_L) : $[-5, 5]$ V;
c-ii) input voltage rate $(\dot{u}_R, \dot{u}_L)$: $[-2, 2]$ V s^{-1};
c-iii) motor current $(v_{\mathfrak{q}_L}, v_{\mathfrak{q}_R})$: $[-3, 3]$ A;
c-iv) tilt angle (α): $[-15, 15]^\circ$;
c-v) heading angle rate (v_θ): $[-120, 120]^\circ$/s.

In our experiments, the WIP follows a figure *eight knot* and a certain *zig-zag* path; a concatenated path for smooth transition of the WIP between *eight knot* and *zig-zag* path is shown in Fig. 5. In particular, seven intermediate points are prescribed on the *eight knot* at a distance of 1.41 m between them and seventeen intermediate points are prescribed on the *zig-zag* path at a distance of 0.35 m between them.

The discrete-time optimal control problem for the variational integrator[4] (13) with control constraints (c-i)-(c-ii) and state constraints (c-iii)-(c-v) is given by

$$\underset{\{u_k, v_{s_k}\}_{k=0}^{N-1}}{\text{minimize}} \ \mathbb{J}(u, v_s) := \frac{1}{2}\sum_{k=0}^{N-1} (u_R)_k (v_{\mathfrak{q}_R})_k + (u_L)_k (v_{\mathfrak{q}_L})_k$$

subject to

$$\begin{cases} \text{system dynamics (13)} \\ -5 \leq (u_R)_k, (u_L)_k \leq 5 \end{cases} \quad \text{for } k \in [N-1]$$

$$\begin{cases} -3 \leq (v_{\mathfrak{q}_L})_k, (v_{\mathfrak{q}_R})_k \leq 3 \\ -\frac{\pi}{12} \leq \alpha_k \leq \frac{\pi}{12} \\ -\frac{2\pi}{3} \leq (v_\theta)_k \leq \frac{2\pi}{3} \\ -2h \leq (u_R)_{k-1} - (u_R)_k \leq 2h \\ -2h \leq (u_L)_{k-1} - (u_L)_k \leq 2h \\ g_k = \bar{g}_{k_j} \text{if } k = k_j \text{ for any } j = 1, \ldots, N_m \end{cases}$$

$$\text{for } k = 1, \ldots, N-1$$

$$(g_0, \alpha_0, (v_s)_0) = (\bar{g}_0, \bar{\alpha}_0, (\bar{v}_s)_0)$$

$$(g_N, \alpha_N, (v_s)_N) = (\bar{g}_N, \bar{\alpha}_N, (\bar{v}_s)_N) \tag{14}$$

where $(\bar{g}_0, \bar{\alpha}_0, (\bar{v}_s)_0)$, $(\bar{g}_N, \bar{\alpha}_N, (\bar{v}_s)_N)$ and the sequence $\{\bar{g}_{k_j}\}_{k_j=1}^{N_m} \subset G$ are fixed.

Remark 2: Note that the optimal trajectories are synthesized by solving the discrete-time optimal control problem (14) using IPOPT solver [28] that is integrated into MATLAB with the help of a symbolic computation toolbox CasADi [29]. We employ a direct optimization technique for solving the optimal control problem (14) here. It should be noted that there is an alternative of employing an indirect method by utilizing the techniques in [30], which may be more accurate [31].

The figures *eight knot* and *zig-zag* paths are employed as benchmarks to test our numerical algorithms. The following optimization parameters have been used for simulating the constrained optimal trajectories:

1) step length (h): 5 ms;
2) final time (T):
   a) *eight knot:* 21.175 s;
   b) *zig zag:* 19.36 s;
   c) complete trajectory: 79.3150 s;
3) number of Steps $(N = T/h)$:
   a) *eight knot:* 4235;
   b) *zig zag:* 3872;
   c) complete trajectory : 15864.

These simulated trajectories have been further validated by experiments.

[3]Note that the Jacobian of the left hand side of (13c) is linear in states v_s. and the system is inherently unstable.

[4]Note that there are no constraints on charge at the motor terminals and wheel angles. Therefore, discrete evolution of these states in (13b) is neglected for the optimization.

C. Current Dynamics and Computation Time

Let us further elaborate on the role of current dynamics in designing optimal trajectories.

1) Optimization and Current Dynamics: When the current dynamics are fast enough to reach steady state in the considered sampling time h, the current dynamics could be replaced with algebraic constraints. The algebraic constraints are defined by the last two equations for the current dynamics of the WIP (see (23) in Appendix C) with setting its left-hand side to zero. Note that these algebraic constraints render the motor current as an explicit map of input voltage and the remaining states. Therefore, we get the WIP dynamics without the current, by neglecting the last two equations of the dynamics (13). This can be done by replacing the motor current with the explicit map in the dynamics (13). Since we neglected the current dynamics, the dimension of the WIP dynamics without the current will reduce by two.

Note that the current dynamics modeling is essential due to the fact that it simplifies the control architecture. If the torque is considered as a plant input to the WIP then a cascaded control architecture is needed. The inner-loop controller will regulate the torque with voltage as its plant input and the outer loop then will facilitate the WIP motion with torque inputs. The inner-loop controller is subject to input saturations (battery voltage) and current limits of the motor drive. Therefore, accounting such constraints while designing optimal trajectories demands modeling of the current dynamics. In addition, the WIP model with current dynamics also allows a simple control architecture in which a single controller enables seamless WIP motion.

2) Computation Time: In literature, the optimal control problem (14) is solved in a standard way in which the variational integrator (13) in (14) is replaced with a discrete-time approximation of the continuous-time WIP dynamics [see (23) in Appendix C]. The continuous-time system dynamics are typically approximated in discrete time by employing various numerical techniques such as RK1, RK2, RK4, where RKn is the fixed time step Runge–Kutta method of nth order. We have conducted a comparative study of the computation time of solving (14) with techniques RK1, RK2, RK4, and variational integrator (VarInt). All integration techniques are initialized with the same set of initial conditions and use the step length of 5 ms as time step. The relative convergence tolerance parameter considered for IPOPT is 10^{-4}. The optimal control problem (14) for *eight* knot and *zig-zag* path (see Fig. 5) is solved on a machine with processor - Intel(R) Core(TM) i7-8700 CPU @ 3.20 GHz, RAM - 8 GB, operating system - Windows 10 64-Bit, MATLAB 2019a in integration CasADi v3.2.3, and the computation time is reported in Fig. 3. It is observed that the computation time of the variational integrator is comparable to the first order technique RK1 and is less as compared to other higher order schemes such as RK2, RK4 (see Fig. 3). It is worth noting that the computation time of (14) is influenced by the choice of way points, initial guesses for the solver, and optimization parameters like solver tolerance.

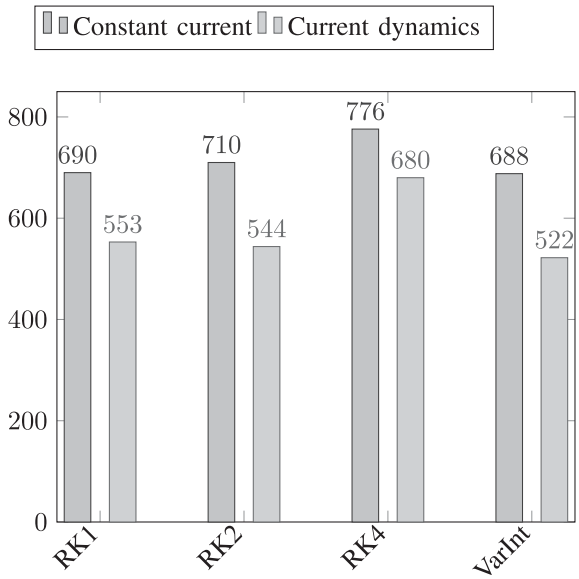

Fig. 3. Computation time comparison. Constant current denotes the case in which the current dynamics is replaced with algebraic constraints.

TABLE I
WIP MODEL PARAMETERS

Symbol	Value	Description
g	$9.81\,\mathrm{m\,s^{-2}}$	gravity constant
m_b	$277 \cdot 10^{-3}\,\mathrm{kg}$	body mass
I_B		body inertia
I_{Bxx}	$543.108 \cdot 10^{-6}\,\mathrm{kg\,m^2}$	about the x-axis
I_{Byy}	$481.457 \cdot 10^{-6}\,\mathrm{kg\,m^2}$	about the y-axis
I_{Bzz}	$153.951 \cdot 10^{-6}\,\mathrm{kg\,m^2}$	about the z-axis
m_w	$28 \cdot 10^{-3}\,\mathrm{kg}$	wheel mass
I_W		wheel inertia
I_{Wxx}	$4.957 \cdot 10^{-6}\,\mathrm{kg\,m^2}$	about the x-axis
I_{Wyy}	$7.411 \cdot 10^{-6}\,\mathrm{kg\,m^2}$	about the y-axis
I_{Wzz}	$4.957 \cdot 10^{-6}\,\mathrm{kg\,m^2}$	about the z-axis
l	$48.67 \cdot 10^{-3}\,\mathrm{m}$	distance from wheel axis to body center of mass
r_w	$33 \cdot 10^{-3}\,\mathrm{m}$	wheel radius
$2d_w$	$2 \times 49 \cdot 10^{-3}\,\mathrm{m}$	distance between wheels
d_v	$1.532 \cdot 10^{-3}\,\mathrm{N\,m\,rad^{-1}}$	viscous damping coefficient
d_c	$32.6 \cdot 10^{-3}\,\mathrm{N\,m}$	coulomb damping coefficient
d_0	$8-$	slope of the damping curve
I_M	$268.528 \cdot 10^{-9}\,\mathrm{kg\,m^2}$	inertia motor shaft
I_G	$1.807 \cdot 10^{-6}\,\mathrm{kg\,m^2}$	inertia gear stage
n_{wm}	$(78/11)^2-$	gear ratio wheel to motor
n_{wg}	$78/11-$	gear ratio wheel to gear
k_e	$3.76 \cdot 10^{-3}\,\mathrm{V/(rad\,s)}$	motor back emf constant
k_m	$3.76 \cdot 10^{-3}\,\mathrm{N\,m\,A^{-1}}$	motor torque constant
L_m	$4 \cdot 10^{-4}\,\mathrm{H}$	motor inductance
R_m	$1.5\,\Omega$	motor resistance

IV. EXPERIMENTS

The WIP (see Fig. 1) is an experimental setup developed at Technical University of Munich,[5] for research [32], teaching and demonstration purposes. The model parameters (see Table I) have been derived from the CAD model of the robot and further validated by conducting experiments on the setup. The simulation results of the identified model demonstrate a high degree of congruence with the experimental data.

[5]The WIP shown in Fig. 1 has been developed, build and modeled by Klaus Albert together with several students writing their term- and master's thesis on the project.

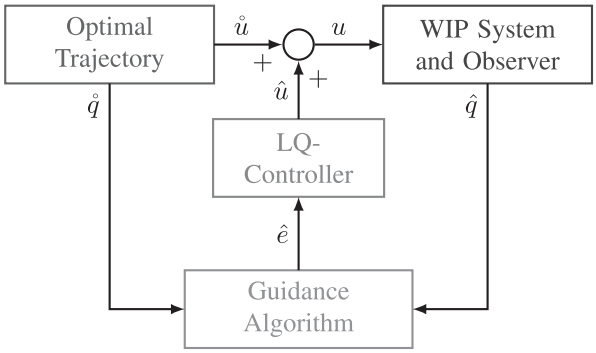

Fig. 4. Closed-loop WIP system.

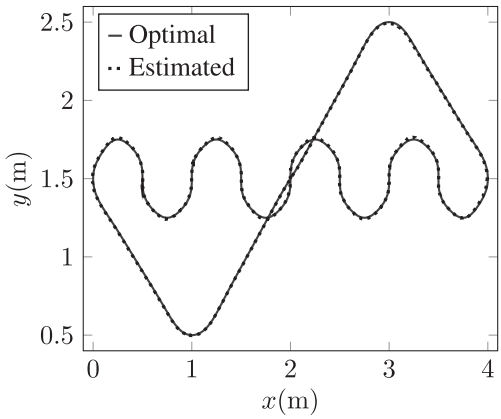

Fig. 5. Phase portrait on the x-y plane.

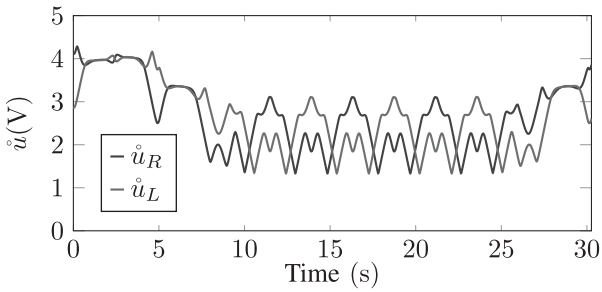

Fig. 6. Feedforward control action.

A. WIP System Description

The WIP weights 333 g, has a height of 195 mm and a width of 103 mm. Most of the parts of the robot are 3D printed. The wheels of the robot are driven by two brushed 6 W dc electric motors mounted on the main body of the robot. The motors are connected to wheels via two stage gears with the total gear ratio from the motor shafts to the wheels equal to 50.28. The motors are connected to two H-bridges motor driver DRV8835 from Texas Instruments, which limit the motor current to a maximum of 3 A. A lithium polymer battery of 7.4 V nominal voltage is fitted onboard to provide energy to the sensors, electronics, and motor drives. The electronic circuit board fitted onboard comes with a 32-bit microcontroller AT32UC3C1512 C from Atmel that runs at 66 MHz, a Bluetooth module to bridge the communication between the PC and the microcontroller, a three-axis accelerometer ADXL345 from analog devices to measure the body acceleration and the acceleration due to gravity, and a three-axis gyroscope ITG-3050 from InvenSense to measure the angular rate of the body. In addition, two optical encoders of 900 counts per revolution (cpr) are fitted on each wheel to measure the relative differences between the body tilt angle α and the wheel angles ϕ_R and ϕ_L, and these encoders are evaluated by two quadrature decoders on the microcontroller, which leads to an effective resolution of 3600 cpr. The onboard sensors provide the rate measurements and the body tilt angle measurements. However, the absolute measurements of the robot position and its orientation on the x-y plane is not possible with the onboard sensors, and an optical tracking system, Vicon with 10 Vera v1.3 cameras covering a tracking area of $4 \times 6.5\,\mathrm{m}$, provides the position and the orientation measurements via Bluetooth to the robot controller. The Vicon system runs at a sampling rate of 50 Hz and the controller generates its digital control sequences for the motor drives at a sampling rate of 5 ms.

B. Experimental Results

The trajectory tracking system for the WIP consists of a feedforward input $\mathring{u}$ and the corresponding state trajectory $\mathring{q}$ that are generated offline by solving a discrete-time optimal control problem (14), and an onboard closed-loop input $\hat{u}$ computed from an LQR to mitigate unaccounted disturbances and to maintain stability of the system, as shown in Fig. 4. The derivation of the linear discrete-time model may be found in Appendix C and Appendix D, and the design of the LQR, the observer and the guidance algorithm may be found in Appendix E. We experimented with two trajectories: the figure *eight knot* and a *zig-zag* path. During the experiments, both trajectories were concatenated to allow the robot to transit from one trajectory to another smoothly. For demonstration purposes, we have truncated the state-action trajectory to 30.3 s in which the robot moves along the figure *eight knot* starting at $(1, 0.5)$ in the x-y plane and switches to the *zig-zag* path at the location $(4, 1.5)$ in x-y plane, as shown in Fig. 5. We have included a supplementary MPEG-4 video file that contains a video of the experiments along with a synchronized animation of Fig. 5.[6] The corresponding optimal control profile for the maneuver is shown in Fig. 6. It is evident from Fig. 5 that the robot follows the reference trajectory very well in linear motion. The peak deviations from the reference occur while executing sharp turns at high speed due to unmodeled disturbances, sensor noise, and communication delays. The robot moves on the straight lines with velocities up to $0.6\,\mathrm{m\,s^{-1}}$ followed by 90° turns and *zig-zag* curves with high heading rates up to $\frac{2\pi}{3}\,\mathrm{rad\,s^{-1}}$ at velocities around $0.3\,\mathrm{m\,s^{-1}}$. The tracking error in x, y as well as θ is plotted in Fig. 7. The maximum/root-mean-square (rms) error (observed during the experiments) in the position (x, y) is 24 mm / 8.3 mm and in orientation (θ) is 12.1° / 3.2°. The position and the orientation of the robot are estimated based on

[6][Online]. Available: http://ieeexplore.ieee.org

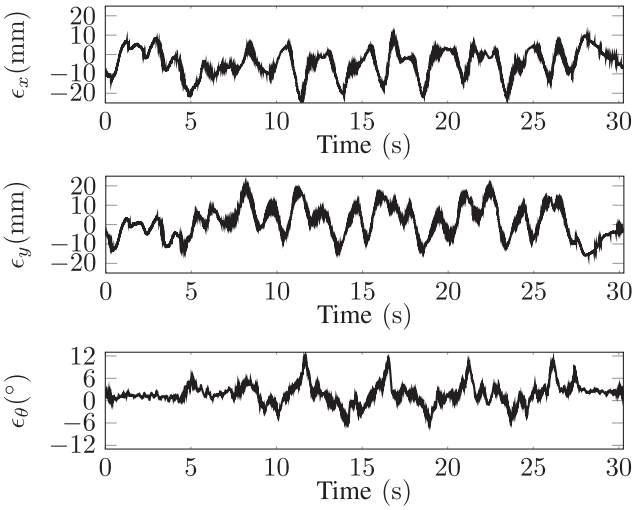

Fig. 7. Tracking error in x, y, and θ.

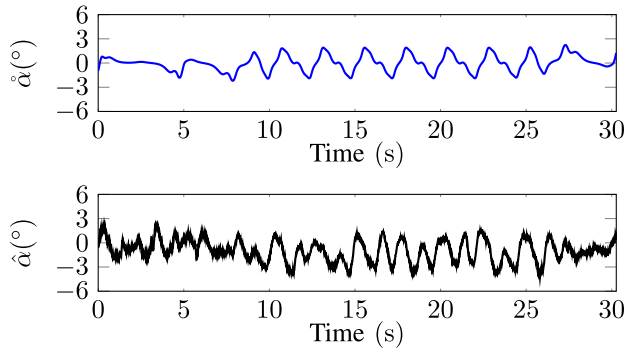

Fig. 8. Optimal tilt angle $\mathring{\alpha}$ and estimated tilt angle $\hat{\alpha}$.

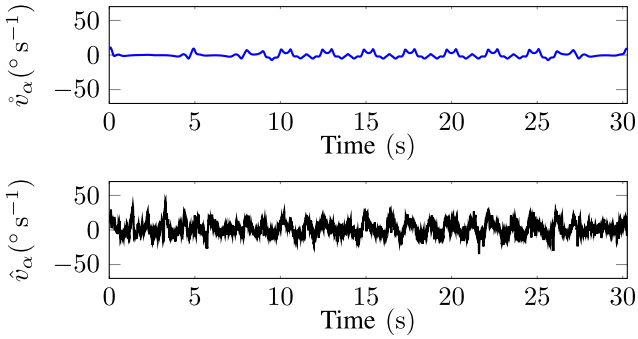

Fig. 9. Optimal tilt rate $\mathring{v}_\alpha$ and estimated tilt rate $\hat{v}_\alpha$.

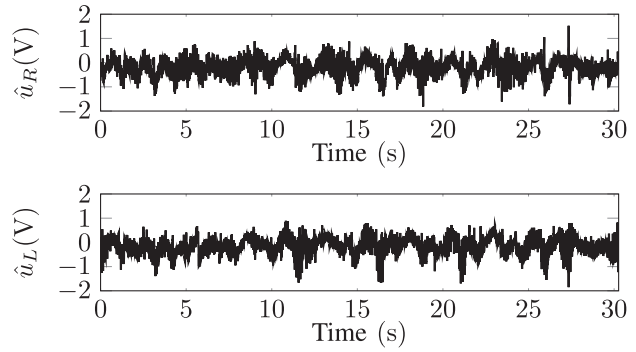

Fig. 10. Feedback control action ($\hat{u}$).

the data received from the Vicon tracking system. The difference in the sampling rate of the controller (5 ms) and the Vicon system (20 ms) necessitate the robot observer to predict the robot position and the orientation without measurement update steps unless the position and orientation measurements are received from the tracking system.

As mentioned previously, a LQR is employed for the stabilization of the system and compensation of disturbances due to system nonlinearities, friction, and communication delays over the wireless network. Note that the system is highly nonlinear and stabilization of the tilt angle α (see Fig. 8) requires sharp control responses from the controller as shown in Fig. 10. In order to execute a fast forward motion, the robot tilts up to 5° during maneuvers (see Fig. 8) and the tilt rate goes up to 41°s^{-1}. During the maneuvers with high tilt angle and tilt rate (see Fig. 9) the controller response reaches 1.9 V for maintaining stability, and a response of 0.4Vrms during the stable motion, i.e., when the tilt angle and tilt rate are nearly zero (see Fig. 10).

V. Conclusion

In this article, we derived a discrete-time model of the WIP system using a structure preserving discretization scheme and generated optimal trajectories for the robot by solving a discrete-time constrained optimal control problem. We then conducted experiments in which the optimal state trajectory was provided as a reference to the robot with the optimal control trajectory as a feedforward control action and found a high degree of congruence in the optimal trajectory and the estimated trajectory of the robot. These experiments established the validity of the proposed model and the proposed tracking control strategy. Finally, these experiments throw light on the nonlinear nature of the WIP system since the stability in the tilt motion can only be achieved by motion on the x-y plane and, therefore, tracking a reference trajectory while maintaining stability is quite challenging.

Appendix A
Nonholonomic Systems: Overview

Let us discuss some key concepts required in deriving discrete-time variational integrators for nonholonomic systems: We begin with constrained distributions and reduced Lagrangians, followed by a discussion on the nonholonomic connection and its local form. We give a catalog of concepts from classical mechanics below; a wealth of information about the geometry of nonholonomic systems may be found in [26], [33], and [34].

A. Lagrangian and Constrained Distributions

Let Q be the configuration space of a nonholonomic mechanical system and let G be a Lie group. Suppose

$$G \times Q \ni (\bar{g}, q) \mapsto \Phi_{\bar{g}}(q) \in Q$$

be a group action of the Lie group G on the manifold Q. Then, the space of symmetries at a given configuration $q \in Q$ is the orbit of G

$$\mathrm{Orb}_G(q) := \{\, \Phi_{\bar{g}}(q) \mid \bar{g} \in G \}$$

and it is a submanifold [33, p. 107] of Q. Let $\mathfrak{g}$ be the Lie algebra of the Lie group G and

$$\xi_Q(q) := \left. \frac{d}{d\epsilon} \right|_{\epsilon=0} \Phi_{\mathrm{e}(\epsilon\xi)}(q)$$

be the infinitesimal generator of $\xi \in \mathfrak{g}$. Then, the tangent space of the orbit at a point q is given as

$$T_q \mathrm{Orb}_G(q) = \{\xi_Q(q) \mid \xi \in \mathfrak{g}\}.$$

Let $TQ \ni (q, v_q) \mapsto L(q, v_q) \in \mathbb{R}$ be the Lagrangian of the nonholonomic system with a regular distribution[7] $\mathcal{D}$ satisfying nonholonomic constraints.

The following assumptions, standard in the literature [26], [33], [34], have been imposed throughout.

A-i) The Lagrangian L is invariant under the group action Φ, i.e., for all $\bar{g} \in G$ and $q \in Q$

$$L(q, v_q) = L\left(\Phi_{\bar{g}}(q), T_q\Phi_{\bar{g}}\left(v_q\right)\right).$$

A-ii) The distribution $\mathcal{D}$ is invariant under the group action, i.e., the subspace $\mathcal{D}_q \subset T_qQ$ is translated under the tangent lift of the group action to the subspace $\mathcal{D}_{\Phi_{\bar{g}}(q)} \subset T_{\Phi_{\bar{g}}(q)}Q$ for all $\bar{g} \in G$ and $q \in Q$.

A-iii) For each $q \in Q$, $T_qQ = \mathcal{D}_q + T_q\mathrm{Orb}_G(q)$.

Assumption (A-i) is the key property needed to define the reduced Lagrangian below and (A-ii) is necessary to define the local form of the nonholonomic connection that is discussed in Appendix A-B.

Let a principal fiber bundle [35] $Q := G \times M$ be the configuration space of a mechanical system with G as a Lie group, and M as a manifold that defines the shape space or the base manifold. Let $q := (g, s)$ be a configuration on the manifold $G \times M$. Then, the reduced Lagrangian is defined as

$$\begin{aligned} TM \times \mathfrak{g} \ni\ & (s, v_s, \xi) \mapsto L^\flat\left(s, v_s, \xi\right) \\ & := L\left((e, s), \left(T_g\Phi_{g^{-1}}\left(v_g\right), v_s\right)\right) \in \mathbb{R} \end{aligned} \tag{15}$$

where

$$\xi = T_g\Phi_{g^{-1}}\left(v_g\right) \in \mathfrak{g}.$$

B. Nonholonomic Connection (See [26], [35] for Details)

Let $\mathcal{V}_q$ be the space of tangent vectors parallel to the symmetric directions (i.e., the vertical space), $\mathcal{D}_q$ be the space of velocities satisfying the nonholonomic constraints at a given configuration q, $\mathcal{S}_q$ be the space of symmetric directions satisfying nonholonomic constraints (4), and $\mathcal{H}_q$ be a space of tangent vectors satisfying nonholonomic constraints but not aligned with the symmetric directions. Then, these subspaces of T_qQ are identified as

$$\mathcal{V}_q = T_q\mathrm{Orb}_G(q), \quad \mathcal{S}_q = \mathcal{V}_q \cap \mathcal{D}_q, \quad \mathcal{D}_q = \mathcal{S}_q \oplus \mathcal{H}_q.$$

Definition 1: A principal connection $\mathcal{A} : TQ \to \mathfrak{g}$ is a Lie algebra valued one form that is linear on each subspace and satisfies the following conditions:

1) $\mathcal{A}(q) \cdot \xi_Q(q) = \xi$, $\xi \in \mathfrak{g}$, and $q \in Q$;
2) $\mathcal{A}$ is equivariant:

$$\mathcal{A}\left(\Phi_g(q)\right) \cdot T_q\Phi_g\left(v_q\right) = \mathrm{Ad}_g\left(\mathcal{A}(q) \cdot v_q\right)$$

for all $v_q \in T_qQ$ and $g \in G$, where Φ_g denotes the group action of G on Q and Ad_g denotes the adjoint action of G on $\mathfrak{g}$.

The principal connection determines a unique Lie algebra element corresponding to a tangent vector $v_q \in T_qQ$. For a given vertical space $\mathcal{V}_q$ and a horizontal space $\mathcal{H}_q$, a vector $v_q \in T_qQ$ can be uniquely represented as $v_q = \mathrm{ver}(v_q) + \mathrm{hor}(v_q)$, where $\mathrm{ver}(v_q) \in \mathcal{V}_q$ and $\mathrm{hor}(v_q) \in \mathcal{H}_q$. By the definition of the principal connection

$$\mathcal{A}(q) \cdot \mathrm{ver}\left(v_q\right) = \xi$$

where $\xi \in \mathfrak{g}$ is the unique Lie algebra element associated with the vertical component $\mathrm{ver}(v_q)$, i.e., $\mathrm{ver}(v_q) = \xi_Q(q) \in T_qQ$ for some $\xi \in \mathfrak{g}$. Consequently, the connection evaluates to zero on the horizontal component $\mathrm{hor}(v_q)$, i.e.,

$$\mathcal{A}(q) \cdot \mathrm{hor}\left(v_q\right) = 0.$$

If the configuration space is a principle fiber bundle $Q = G \times M$, the principle connection admits a local form $\mathbb{A} : TM \to \mathfrak{g}$ such that the principle connection in terms of the local form is given by [35]

$$\mathcal{A}(q) \cdot v_q = \mathrm{Ad}_g\left(g^{-1}(v_g) + \mathbb{A}(s)v_s\right)$$

for all $q := (g, s) \in Q$ and $v_q := (v_g, v_s) \in T_qQ$, where $g^{-1}(v_g)$ is the tangent lift of the left action of g^{-1} on $g \in G$, and $\mathrm{Ad}_g : \mathfrak{g} \to \mathfrak{g}$ is given by

$$\mathrm{Ad}_g(\xi) := \left. \frac{d}{d\epsilon} \right|_{\epsilon=0} g\,\mathrm{e}(\epsilon\xi)g^{-1} \quad \text{for all } \xi \in \mathfrak{g}.$$

For mechanical systems evolving on principle fiber bundles, in general, the base space M corresponds to the set of configurations that are directly controlled by the control forces. Hence, a path on the base space can be followed by applying these forces. A path on the fiber space G is constructed by fiber velocities at given fiber configurations. These fiber velocities are uniquely related to the nonholonomic momentum and the base velocities via a nonholonomic connection. Let us pick, for $q \in Q$, a vector subspace $\mathcal{U}_q \subset \mathcal{V}_q$ such that

$$\mathcal{V}_q = \mathcal{S}_q \oplus \mathcal{U}_q$$

where $\mathcal{S}$ is a distribution consists of the symmetric horizontal directions.

[7] Recall that a smooth distribution $\mathcal{D}$ on a manifold Q is a smooth assignment of subspaces $\mathcal{D}_q \subset T_qQ$ at each $q \in Q$. A distribution is said to be *regular* [33, p. 96] on Q if there exists an integer d such that $\dim(\mathcal{D}_q) = d$ for all $q \in Q$.

Definition 2 ([35, Definition 6.2 on p. 38]): Assume that the Assumption (A-iii) holds. Then, the nonholonomic connection $A^{\text{nhc}} : TQ \to \mathcal{V}$ is a vertical valued one form whose horizontal space at $q \in Q$ is the orthogonal complement of the subspace $\mathcal{S}_q$ in $\mathcal{D}_q$ and satisfies the following:

$$A^{\text{nhc}} := A^{\text{kin}} + A^{\text{sym}}$$

where $A^{\text{kin}} : TQ \to \mathcal{U}$ is the kinematic connection enforcing nonholonomic constraints and $A^{\text{sym}} : TQ \to \mathcal{S}$ is the mechanical connection corresponding to symmetries in the constrained direction.

The kinematic connection A^{kin} and the mechanical connection A^{sym} satisfy the following conditions:

$$A^{\text{kin}}(q) \cdot v_q = 0 \quad \text{for all } v_q \in \mathcal{D}_q$$
$$A^{\text{sym}}(q) \cdot v_q = v_q \quad \text{for all } v_q \in \mathcal{S}_q.$$

Remark 3: If the distribution $\mathcal{S}_q$ and the horizontal distribution are invariant under the group action, then the nonholonomic connection is a principal connection.

In case the nonholonomic connection is a principal connection, the connection is represented as

$$\text{Ad}_g \left(g^{-1}(v_g) + \mathbb{A}(s) v_s \right) = \text{Ad}_g \left(\Omega \right)$$

where

$$\Omega \in \mathfrak{s}_s := \{ \xi \in \mathfrak{g} \mid \xi_Q(q) \in \mathcal{S}_q \}$$

is the *locked angular velocity*, i.e., the velocity achieved by locking the joints represented by the base configuration variable. This local form of the nonholonomic connection can be written as

$$g^{-1}(v_g) + \mathbb{A}(s) v_s = \Omega. \tag{16}$$

For the principal kinematic case, i.e., $\mathcal{S}_q = \mathcal{D}_q \cap \mathcal{V}_q = \{0\}$ for all $q \in Q$, the local form of the nonholonomic connection (16) simplifies to

$$g^{-1}(v_g) + \mathbb{A}(s) v_s = 0. \tag{17}$$

Therefore, for a smooth curve $\mathbb{R} \ni t \mapsto (g(t), s(t)) \in G \times M$, the group motion can be constructed by the nonholonomic connection for a given base trajectory as

$$\dot{g}(t) = -g(t) \mathbb{A} \left(s(t) \right) \dot{s}(t).$$

APPENDIX B
DISCRETE-TIME VARIATIONAL INTEGRATOR

Equipped with necessary geometric notions, in particular, the reduced Lagrangian and the local form of the nonholonomic connection, we are in a position to state the discrete-time reduced Lagrange-D'Alembert-Pontryagin nonholonomic principle [26] to derive the variational integrators for nonholonomic principal kinematic systems.

Recall that $[N] := \{0, \ldots, N\}$. Define a discrete path

$$[N] \ni k \mapsto (s_k, v_{s_k}, g_k) := (s(t_k), v_s(t_k), g(t_k)) \in TM \times G \tag{18}$$

on the reduced space that satisfies the following constraints:

$$s_{k+1} - s_k = h v_{s_k}, \quad g_{k+1} = g_k \varphi(-h \mathbb{A}(s_k) v_{s_k})$$

where h is the time difference between any two consecutive configurations, i.e., $t_{k+1} - t_k = h$, and the map $\varphi : \mathfrak{g} \to G$ represents the *difference* between two system configurations defined by Lie group elements by a unique element in its Lie algebra.

In most of the cases, φ is taken to be the exponential map $\text{e} : \mathfrak{g} \to G$ that is a diffeomorphism in the neighborhood $\mathcal{O}_e \subset G$ of the group identity $e \in G$ [36, p. 256]. The map e serves the purpose of φ because the consecutive group configurations g_k and g_{k+1} do not differ by a large value, i.e., $g_k^{-1} g_{k+1} \in \mathcal{O}_e \subset G$ for any discrete-time instant k. Furthermore, the discrete control force

$$[N] \ni k \mapsto \tau_k := \tau(t_k) \in T^*M$$

is an approximation of the continuous-time force τ controlling the shape of the dynamics.

Definition 3: The discrete reduced LDAP principle for principal kinematic systems

$$\delta \sum_{k=0}^{N-1} L^\flat \left(s_k, \frac{s_{k+1} - s_k}{h}, \frac{\varphi^{-1}(g_k^{-1} g_{k+1})}{h} \right) + \langle \tau_k, s_k \rangle = 0$$

subject to

nonholonomic constraints: $g_{k+1} = g_k \varphi(-h \mathbb{A}(s_k) v_{s_k})$

and,

horizontal variations: $\left(g_k^{-1} \delta g_k, \delta s_k \right) = \left(-\mathbb{A}(s_k) \delta s_k, \delta s_k \right).$

The discrete reduced LDAP principle leads to the following sets of discrete-time equations:

$$\begin{aligned}
&s_{k+1} = s_k + h v_{s_k} \\
&g_{k+1} = g_k \varphi(-h \mathbb{A}(s_k) v_{s_k}) \\
&\frac{\partial L_k^\flat}{\partial v_s} - h \frac{\partial L_k^\flat}{\partial s} - \left(\varphi_{-v_{s_k}} \circ \mathbb{A}(s_k) \right)^* \left(\frac{\partial L_k^\flat}{\partial \xi} \right) \\
&= \frac{\partial L_{k-1}^\flat}{\partial v_s} - \left(\varphi_{v_{s_{k-1}}} \circ \mathbb{A}(s_{k-1}) \right)^* \left(\frac{\partial L_{k-1}^\flat}{\partial \xi} \right) + h \tau_{k-1}
\end{aligned} \tag{19}$$

where

$$\varphi_{v_{s_k}} := T\varphi^{-1} \left(\varphi(-h \mathbb{A}(s_k) v_{s_k}) \right) \circ \varphi(-h \mathbb{A}(s_k) v_{s_k})$$

is the right translated tangent lift of the local diffeomorphism φ^{-1}, and

$$L_k^\flat := L^\flat \left(s_k, (s_{k+1} - s_k)/h, \varphi^{-1}(g_k^{-1} g_{k+1})/h \right)$$

is the reduced Lagrangian (15).

APPENDIX C
NONLINEAR STATE-SPACE MODEL

The nonlinear state-space model of the WIP is derived using first order modeling as discussed in [37]. We derive a more comprehensive WIP model than the existing literature [21], [37] based on the fact that we have included the dynamics of the currents at the modeling stage instead of modeling it as a separate

system and then connecting it to the mechanical system. Let

$$A := \begin{pmatrix} -\sin\theta & \cos\theta & 0 & 0 & 0 & 0 & 0 & 0 \\ \cos\theta & \sin\theta & d_w & 0 & -r_w & 0 & 0 & 0 \\ \cos\theta & \sin\theta & -d_w & 0 & 0 & -r_w & 0 & 0 \end{pmatrix}$$

be a connection matrix such that $A\dot{q} = 0$ defines the nonholonomic constraints (3). Then, the Euler–Lagrange equations for the Lagrangian (5) of the nonholonomic system with nonholonomic constraints (3) and external forcing (6) is given by

$$\frac{d}{dt}\left(\frac{\partial L}{\partial \dot{q}}\right) - \frac{\partial L}{\partial q} = \mathcal{F} + A^{\intercal}\lambda$$
$$A\dot{q} = 0 \tag{20}$$

where $\lambda \in \mathbb{R}^3$ is a vector of Lagrange multipliers and $\mathcal{F}$ accounts for the dissipative and external forcing to the system. Furthermore, the Euler–Lagrange equations (20) are simplified in terms of the kinetic energy T and the potential energy V as

$$\underbrace{\frac{\partial^2 T}{\partial \dot{q}^2}}_{M}\ddot{q} + \underbrace{\frac{\partial^2 T}{\partial \dot{q}\partial q}\dot{q} - \frac{\partial T}{\partial q}}_{K} \underbrace{-\frac{\partial^2 V}{\partial \dot{q}\partial q}\dot{q} + \frac{\partial V}{\partial q}}_{P} = \mathcal{F} + A^{\intercal}\lambda \tag{21a}$$

$$A\dot{q} = 0 \tag{21b}$$

where M is the mass matrix. For geometric insight, let us define heading rate v_θ and forward velocity v_d as

$$v_d = \frac{r_w}{2}(\dot{\phi}_R + \dot{\phi}_L)$$
$$v_\theta = \frac{r_w}{2d_w}(\dot{\phi}_R - \dot{\phi}_L).$$

Note that the nonholonomic constraints in (21) define permissible velocities of the WIP. Therefore, to define the equations of motion of the system in minimal coordinates without nonholonomic constraints, let us consider

$$\dot{q} = S\nu \tag{22}$$

where

$$\nu := (v_\alpha, v_d, v_\theta, v_{\mathfrak{q}_R}, v_{\mathfrak{q}_L})^{\intercal}$$

and

$$S = \begin{pmatrix} 0 & \cos\theta & 0 & 0 & 0 \\ 0 & \sin\theta & 0 & 0 & 0 \\ 0 & 0 & 1 & 0 & 0 \\ 1 & 0 & 0 & 0 & 0 \\ 0 & \frac{1}{r_w} & \frac{d_w}{r_w} & 0 & 0 \\ 0 & \frac{1}{r_w} & -\frac{d_w}{r_w} & 0 & 0 \\ 0 & 0 & 0 & 1 & 0 \\ 0 & 0 & 0 & 0 & 1 \end{pmatrix}$$

lies in the null space of the matrix A. Now, the Lagrange multipliers λ in (21) are eliminated by premultiplying both sides in (21a) by $S^{\intercal}$. Then, substituting $\dot{q} = S\nu$ and $\ddot{q} = S\dot{\nu} + \dot{S}\nu$ to (21) leads to

$$\dot{\nu} = -(S^{\intercal}MS)^{-1}S^{\intercal}\left(M\dot{S}\nu + K + P - \mathcal{F}\right).$$

Finally, neglecting the kinematics for the states $\phi_L, \phi_R, \mathfrak{q}_L, \mathfrak{q}_R$ in (22), the system dynamics is written on the reduced space in terms of the new states

$$X := (q_r, \nu)^{\intercal} = ((x, y, \theta, \alpha), (v_\alpha, v_d, v_\theta, v_{\mathfrak{q}_R}, v_{\mathfrak{q}_L}))^{\intercal}$$

as

$$\dot{X} := \begin{pmatrix} S_r\nu \\ -(S^{\intercal}MS)^{-1}S^{\intercal}\left(M\dot{S}\nu + K + P - \mathcal{F}\right) \end{pmatrix} \tag{23}$$

where the reduced matrix S_r is set up by removing last four rows in S.

Appendix D
Linear State-Space Model

We derive a discrete-time linear state-space model of the WIP system for designing the controller and the observer. The linear discrete-time model is derived via linearization of the nonlinear model (23) around $X = 0, u_L = 0, u_R = 0$, and followed by the discretization of the resulting linear model at a sampling rate of 5ms and under the assumption of constant inputs during the sampling interval. In order to avoid high damping due to nonlinear friction, the damping parameters for the linear model are set to $d_v = 4.25 \cdot 10^{-3}$ N m rad^{-1} and $d_c = 0$ Nm. With this set of damping parameters, the linear damping torque curve approximates the nonlinear damping curve well at the nominal operating speed of the system (0.4 m s^{-1}).

Note that due to the linearization at the heading angle $\theta = 0$, the state y is decoupled from the other states and control inputs. Furthermore, the state x in the linear system is the integration of v_d, and hence, to avoid confusion with nonlinear model state x, we denote it by d.

Appendix E
Tracking Controller, Guidance Algorithm and Observer

The WIP is stabilized by an LQR, which is designed for the discrete-time linear model. We have discussed in Appendix D that the linearized discrete-time system does not have access to the states (x, y), but only the traveled forward distance d is available to the controller. Therefore, to facilitate motion of the system on the x-y plane, a guidance algorithm is required for the controller to generate the necessary control actions. The guidance algorithm calculates the control errors for the controller in distance e_d and angle e_θ based on the difference between the current position orientation (x, y, θ) and the desired position orientation (x_d, y_d, θ_d) of a given trajectory. The LQR is calculated using the weighting matrix

$$Q_Y := \text{diag}([1500, \quad 350, \quad 0.1, \quad 0, \quad 0, \quad 1, \quad 0, \quad 0])$$

for the states and

$$R := I_{2\times 2}$$

for the inputs. The state $\hat{q}$ of the robot (see Fig. 4) is estimated by sensor fusion and a model-based observer that suppresses sensor noise besides dealing with communication delays. The

position and the orientation of the robot are estimated based on the data received from the Vicon tracking system over the communication channel with communication time delays in the range between 13 ms to 148 ms with an average time delay of 63 ms. Furthermore, the difference in sampling rate of the controller (5 ms) and the Vicon system (20 ms) as well as possible data package losses requires the robot observer to predict the robot position and its orientation without correction steps unless the position and orientation measurements are available to the observer from the tracking system.

ACKNOWLEDGMENT

The authors would like to thank the students M. Hölzle, C. Leonhardt, F. Kaufmann, T. Wunderlich, V. Priesack, and T. Bürchner, Technical University of Munich who where involved in the development, building, modeling, controller, and observer design process of the WIP with their term- and master's thesis's for their valuable help.

Contribution: K. Albert, F. Anhalt, and B. Lohmann have mainly contributed to the continuous-time modeling, LQR design, trajectory planning, and experiments.

K. Singh Phogat, R. N. Banavar, and D. Chatterjee have mainly contributed to variational integrator modeling, and trajectory planning.

REFERENCES

[1] J. E. Marsden and M. West, "Discrete mechanics and variational integrators," *Acta Numer.*, vol. 10, pp. 357–514, May 2001, doi: 10.1017/S096249290100006X.

[2] K. Pathak, J. Franch, and S. K. Agrawal, "Velocity and position control of a wheeled inverted pendulum by partial feedback linearization," *IEEE Trans. Robot.*, vol. 21, no. 3, pp. 505–513, Jun. 2005.

[3] S. Gajbhiye, R. N. Banavar, and S. Delgado, "Symmetries in the wheeled inverted pendulum mechanism," *Nonlinear Dyn.*, vol. 90, no. 1, pp. 391–403, Oct. 2017, doi: 10.1007/s11071-017-3670-3.

[4] Segway, 2014. [Online]. Available: http://www.segway.com

[5] R. P. M. Chan, K. A. Stol, and C. R. Halkyard, "Review of modelling and control of two-wheeled robots," *Annu. Rev. Control*, vol. 37, no. 1, pp. 89–103, 2013.

[6] F. Grasser, A. D'Arrigo, S. Colombi, and A. C. Rufer, "JOE: A mobile, inverted pendulum," *IEEE Trans. Ind. Electron.*, vol. 49, no. 1, pp. 107–114, Feb. 2002.

[7] Z. Li, C. Yang, and L. Fan, *Advanced Control of Wheeled Inverted Pendulum Systems*. New York, NW, USA: Springer, 2012.

[8] D. Nasrallah, J. Angeles, and H. Michalska, "Velocity and orientation control of an anti-tilting mobile robot moving on an inclined plane," in *Proc. IEEE Int. Conf. Robot. Autom.*, 2006, pp. 3717–3723.

[9] D. Nasrallah, H. Michalska, and J. Angeles, "Controllability and posture control of a wheeled pendulum moving on an inclined plane," *IEEE Trans. Robot.*, vol. 23, no. 3, pp. 564–577, Jun. 2007.

[10] M. Baloh and M. Parent, "Modeling and model verification of an intelligent self-balancing two-wheeled vehicle for an autonomous urban transportation system," in *Proc. Conf. Comput. Intell., Robot., Auton. Syst.*, 2003, pp. 1–7.

[11] A. Blankespoor and R. Roemer, "Experimental verification of the dynamic model for a quarter size self-balancing wheelchair," in *Proc. Amer. Control Conf.*, 2004, vol. 1, pp. 488–492.

[12] A. Salerno and J. Angeles, "The control of semi-autonomous two-wheeled robots undergoing large payload-variations," in *Proc. IEEE Int. Conf. Robot. Autom.*, 2004, vol. 2, pp. 1740–1745.

[13] Y. Kim, S. H. Kim, and Y. K. Kwak, "Dynamic analysis of a nonholonomic two-wheeled inverted pendulum robot," *J. Intell. Robot. Syst.*, vol. 44, no. 1, pp. 25–46, 2005.

[14] S. Kim and S. Kwon, "Nonlinear optimal control design for underactuated two-wheeled inverted pendulum mobile platform," *IEEE/ASME Trans. Mechatronics*, vol. 22, no. 6, pp. 2803–2808, Dec. 2017.

[15] N. R. Gans and S. A. Hutchinson, "Visual servo velocity and pose control of a wheeled inverted pendulum through partial-feedback linearization," in *Proc. IEEE/RSJ Int. Conf. Intell. Robots Syst.*, 2006, pp. 3823–3828.

[16] W. Ye, Z. Li, C. Yang, J. Sun, C.-Y. Su, and R. Lu, "Vision-based human tracking control of a wheeled inverted pendulum robot," *IEEE Trans. Cybern.*, vol. 46, no. 11, pp. 2423–2434, Nov. 2016.

[17] A. Salerno and J. Angeles, "On the nonlinear controllability of a quasi-holonomic mobile robot," in *Proc. IEEE Int. Conf. Robot. Autom.*, 2003, vol. 3, pp. 3379–3384.

[18] H. Vasudevan, A. M. Dollar, and J. B. Morrell, "Design for control of wheeled inverted pendulum platforms," *J. Mechanisms Robot.*, vol. 7, no. 4, 2015, Art. no. 041005, doi: 10.1115/1.4029401.

[19] S. Delgado and P. Kotyczka, "Energy shaping for position and speed control of a wheeled inverted pendulum in reduced space," *Automatica*, vol. 74, pp. 222–229, 2016.

[20] Y. Zhou and Z. Wang, "Robust motion control of a two-wheeled inverted pendulum with an input delay based on optimal integral sliding mode manifold," *Nonlinear Dyn.*, vol. 85, no. 3, pp. 2065–2074, 2016.

[21] S. Kim and S. Kwon, "Dynamic modeling of a two-wheeled inverted pendulum balancing mobile robot," *Int. J. Control, Autom. Syst.*, vol. 13, no. 4, pp. 926–933, Aug. 2015.

[22] K. S. Phogat, R. Banavar, and D. Chatterjee, "Structure-preserving discrete-time optimal maneuvers of a wheeled inverted pendulum," in *Proc. 6th IFAC Workshop Lagrangian Hamiltonian Methods Nonlinear Control LHMNC 2018*, 2018, vol. 51, pp. 149–154, doi: 10.1016/j.ifacol.2018.06.042.

[23] S. Thrun, W. Burgard, and D. Fox, *Probabilistic Robotics*. Cambridge, MA, USA: MIT Press, 2005.

[24] P. M. Esfahani, D. Chatterjee, and J. Lygeros, "Motion planning for continuous-time stochastic processes: A dynamic programming approach," *IEEE Trans. Autom. Control*, vol. 61, no. 8, pp. 2155–2170, Aug. 2016.

[25] D. Wells, "Application of the Lagrangian equations to electrical circuits," *J. Appl. Phys.*, vol. 9, no. 5, pp. 312–320, 1938.

[26] M. Kobilarov, J. E. Marsden, and G. S. Sukhatme, "Geometric discretization of nonholonomic systems with symmetries," *Discrete Continuous Dynamical Syst. Series S*, vol. 3, no. 1, pp. 61–84, 2010.

[27] J. E. Marsden and T. S. Ratiu, *Introduction to Mechanics and Symmetry*. New York, NY, USA: Springer-Verlag, 1994.

[28] A. Wächter and L. T. Biegler, "On the implementation of an interior-point filter line-search algorithm for large-scale nonlinear programming," *Math. Program.*, vol. 106, no. 1, pp. 25–57, 2006, doi: 10.1007/s10107-004-0559-y.

[29] J. Andersson, J. Åkesson, and M. Diehl, "CasADi: A symbolic package for automatic differentiation and optimal control," in *Recent Advances in Algorithmic Differentiation*. New York, NY, USA: Springer, 2012, pp. 297–307.

[30] K. S. Phogat, D. Chatterjee, and R. N. Banavar, "A discrete-time Pontryagin maximum principle on matrix Lie groups," *Automatica*, vol. 97, pp. 376–391, 2018, doi: 10.1016/j.automatica.2018.08.026.

[31] E. Trélat, "Optimal control and applications to aerospace: Some results and challenges," *J. Optim. Theory Appl.*, vol. 154, pp. 713–758, 2012, doi: 10.1007/s10957-012-0050-5.

[32] S. Delgado, "Total energy shaping for underactuated mechanical systems: Dissipation and nonholonomic constraints," Depart. Mech. Eng., Ph.D. dissertation, Tech. Univ. of Munich, Munich, Germany, 2016.

[33] A. M. Bloch, *Nonholonomic Mechanics and Control*. 2nd ed., ser. Interdisciplinary Applied Mathematics. New York, NY, USA: Springer, 2015, vol. 24, with the collaboration of J. Bailieul, P. E. Crouch, J. E. Marsden and D. Zenkov, With scientific input from P. S. Krishnaprasad and R. M. Murray.

[34] J. P. Ostrowski, "The Mechanics and Control of Undulatory Robotic Locomotion," Ph.D. dissertation, California Institute of Technology, 1996.

[35] A. M. Bloch, P. Krishnaprasad, J. E. Marsden, and R. M. Murray, "Nonholonomic mechanical systems with symmetry," *Archive Rational Mech. Anal.*, vol. 136, no. 1, pp. 21–99, 1996.

[36] R. Abraham and J. Marsden, *Foundations of Mechanics*. Providence, RI, USA: AMS Chelsea, 1978.

[37] K. Pathak, J. Franch, and S. K. Agrawal, "Velocity and position control of a wheeled inverted pendulum by partial feedback linearization," *IEEE Trans. Robot.*, vol. 21, no. 3, pp. 505–513, Jun. 2005.

Klaus Albert received the bachelor's degree in mechatronics from the Karlsruhe University of Applied Sciences, Karlsruhe, Germany, in 2009 and the master's degree in mechanical engineering from the Technical University of Munich (TUM), Munich, Germany, in 2012.

He is currently working as a Research Associate with the Chair of Automatic Control at the Department of Mechanical Engineering, TUM. His research interests include Takagi–Sugeno modeling and control, the control of constrained nonlinear systems as well as modeling and control of unstable mobile robots.

Karmvir Singh Phogat received the M.Sc. degree in applied mathematics from Indian Institute of Technology Roorkee, Roorkee, India, in 2012, and the Ph.D. degree in systems and control engineering from the Indian Institute of Technology Bombay, Mumbai, India, in 2018.

He worked with KAIST, South Korea as a Postdoc before joining for another research stint at the University of Tokyo, Japan. His research interests include geometric optimal control and its applications in electrical and aerospace engineering.

Felix Anhalt received the master's degree in mechanical engineering from the Technical University of Munich (TUM), Munich, Germany, in 2016.

Since 2017, he has been working as a Research Associate with the Chair of Automatic Control, TUM. His current research interests include cloud-supported preview control of active suspension systems.

Ravi N. Banavar received the B.Tech. degree in mechanical engineering from the Indian Institute of Technology Madras, Chennai, India, in 1986, the master's degree in mechanical from Clemson University, Clemson, SC, USA, in 1988, and the Ph.D. degree in aerospace from the University of Texas at Austin, Austin, TX, USA, in 1992.

He had a brief teaching stint at UCLA, in 1991–1992, soon after which he joined the Systems and Control Engineering group, Indian Institute of Technology Bombay, in early 1993. He is currently a Professor in this group, and is also a Guest Professor with the Indian Institute of Technology Gandhinagar. He has spent a few sabbatical breaks during his academic career with UCLA (Los Angeles), IISc (Bangalore), and LSS (Supelec, France). His research interests include geometric mechanics, nonlinear and optimal control, with applications to electromechanical and aerospace engineering problems.

Debasish Chatterjee received the Ph.D. degree in electrical engineering from the University of Illinois at Urbana-Champaign, Champaign, IL, USA, in 2007.

He was a Postdoc with ETH Zürich before moving to Indian Institute of Technology Bombay, (IIT Bombay) for service. He is with the Department of Systems and Control Engineering, IIT Bombay. His research interests include constrained control with emphasis on computational tractability, geometric techniques in control, and applied probability.

Prof. Chatterjee was an Associate Editor of Automatica and the IFAC Journal of Systems and Control, and as an Editor of the International Journal of Robust and Nonlinear Control.

Boris Lohmann received the Dipl.-Ing. degree in electrical engineering and the Ph.D. (Dr.-Ing.) degree in electrical engineering from the University of Karlsruhe, Karlsruhe, Germany, in 1987 and 1991, respectively.

He is a Full Professor and the Head of the Chair of Automatic Control with the Department of Mechanical Engineering, Technical University of Munich, Germany. His research interests include linear and nonlinear control systems design, modeling and model reduction, autonomous driving as well as applications in mechatronics and automotive.